Green-aromatic production in typical conditions of fluidized catalytic cracking

Joana F.R. Pinto, Yiu Lau Lam, Marcelo Maciel Pereira, Hugo Cruchade, Alexander Sachse, Ludovic Pinard

Green-aromatic production in typical conditions of fluidized catalytic cracking

Joana Pinto[a], *Yiu Lau Lam*[a] *and Marcelo Maciel Pereira*[a*]

[a]*Instituto de Química – Universidade Federal do Rio de Janeiro, Rio de Janeiro, RJ, Brazil*

Hugo Cruchade[b], *Alexander Sachse*[b], *and Ludovic Pinard*[b]

[b]*Institut de Chimie des Milieux et Matériaux de Poitiers (ICM2P), UMR 7285 CNRS, 4 Rue Michel Brunet, Bâtiment B27, 86073 Poitiers Cedex – France.*

* maciel@iq.ufrj.br

Abstract

The production of green hydrocarbons in the standard refinery has significant potential to reduce our reliance on oil and shorten the path to sustainability. Second-generation biomass can help to achieve this objective yet presents important drawbacks. It is majorly composed of reactive compounds and features low density. These features could be overcome by previously transforming the biomass by ketalization reaction into a bio-crude mainly composed by ketal-sugar derivatives. In this work, a representative compound of the bio-crude class, i.e. 1,2:3,5-di-O-isopropylidene-α-d-xylofuranose (DX) were used in up to 50 wt.% mixtures in *n*-hexane was converted in a laboratory scale fluidized catalytic cracking (FCC) reactor. A commercial and a simplified FCC catalyst were used.

Converting a mixture of 30% DX in *n*-hexane in the presence of a commercial catalyst gave 42.3% aromatics in the liquid product, while pure *n*-hexane gave merely 8.9%. The use of deactivated catalysts further reduced the coke yield to half of the fresh one. The nature of the coke on the spent catalyst is exclusively composed by carbon and hydrogen, demonstrating that DX is easily deoxygenated. The *n*-hexane conversion slight reduced in the presence of DX, and did not reduce the stability of the catalyst through micropore blocking. This work demonstrates that adding DX allows to contributes to high bio-aromatic production in FCC and that products distribution is remarkably affected by the type of catalyst used.

Keywords: Bio-aromatics; Bio-gasoline; FCC; Biomass; Bio-refinery.

1 – Introduction

The green hydrocarbon production in the standard refinery offers great advantages over current alternative approaches to shorten our path to sustainability. Firstly, hydrocarbons have one of the highest combustion enthalpies per volume[1], the higher energy density is a key advantage to reduce transportation costs. Secondly, no new or modifications of legislation are necessary. Thirdly, a giant production and distribution structure of oil industry is available. Finally, besides the great potential to reduce the carbon emission, the possibility to introduce bio-feeds in the refinery may add a stabilizing factor for the oil industry.

There are three main strategies adopted to convert second generation biomass into fuel: organic reaction combined with aqueous phase transformation [2, 3], gasification to CO and H_2 followed by the Fischer-Tropsch process [4, 5]

and thermo-conversion comprising bio-oil production and its transformation in the refinery [6-8]. The first strategy requires a new production structure which is not compatible with existing refineries. The second needs high temperature during gasification [9] and high energetic inputs to revert the entropy involved in the gas formation[5], therefore hindering the application to produce conventional fuel. Nevertheless, it should be pointed out that these two approaches could be used to produce valuable products. The third has several drawbacks, since typical bio-oil contains highly acidic and undesirable products (poly-aromatic and phenol-derivative compounds) that require the addition of significant amounts of hydrogen before their use in standard refineries [7, 10]. This limits the amount of bio-oil to only 5 wt.% in the co-process with gasoil in FCC [11]. Consequently, the economic considerations hinderthe application of green hydrocarbons as refinery feedstock. One further option is the co-process of ethanol and bio-oil derivatives [12, 13], however, ethanol itself is a fuel already.

An alternative route that can potentially overcome the above limitations is the transformation of biomass into a bio-crude by ketalization reaction (using the idea of protective reaction from organic chemistry) [14] followed by catalytic conversion either in a FCC or a hydro conversion unit in fixed-bed reactors.[15] The proposed bio-crude is composed of ketal-sugar derivatives like 1,2:3,5-di-O-isopropylidene-α-d-xylofuranose (DX), 1,2-O-isopropylidene-α-D-xylofuranose, 1,2:5,6-di-O-α-D-Isopropylideneglucofuranose, 1,2:3,5-Di-O-isopropylidene-α-D-xylofuranose and more complex ketal-derivative compounds [16]. Recently this idea to produce such a bio-crude allowed to avoid degradation of carbohydrates during the depolymerisation reaction of wood, however the authors did not realize the potential of this approach to provide an appropriate feed

that could be converted in the regular refineries[17]. Our vision of circular economy is presented in figure 1:

Figure 1: Circular economy for converting second generation biomass into green-hydrocarbons. Sugarcane bagasse, the residue of ethanol and sugar industry, is used as second generation biomass. Emphasis on DX conversion in fluidized catalytic cracking. Firstly, biomass is converted under mild conditions into a bio-crude composed mainly of sugar ketals, among them DX which is a representative compound. The FCC process transforms mixtures of DX in *n*-hexane (up to 50wt.% DX) at 500 ºC in the presence of a commercial catalyst based on faujasite into green mono-aromatics that can be directly used as petrochemicals or mixed with regular fuels like gasoline or jet-fuel.

The catalytic cracking of *n*-hexane is widely used to characterize acid catalysts [18-21] as this linear molecule shows accessibility to medium or even small pores and its conversion requires strong acid sites. The activation of weak σ carbon-carbon and carbon-hydrogen bonds in hydrocarbons was demonstrated under superacidic conditions [21]. The extent of the *n*-hexane reaction rate for the given amount of tetrahedral aluminium in the zeolites can be explained by the Haag's hypothesis of protolytic cracking [22].

In this work, DX, a representative compound of bio-crude, was mixed with up to 50 wt.% in *n*-hexane. These feeds were converted in a laboratory fluidized catalytic reactor under conditions similar to typical FCC processes, in the presence of a commercial and a simplified catalyst, both used and fresh. The simplified catalyst was also deactivated by hydrothermal treatment. The tests were compared with studies conducted under similar conditions with pristine *n*-hexane.

2 – Experimental

Preparation of 1,2:3,5-di-*O*-isopropilidene-β-D-xylofuranose (**DX**). A suspension of the respective anhydrous xylose, (10g) in acetone (volume) was stirred vigorously under ice bath. Sulfuric acid (98%, 0.4 mL) was added in three portions at 5 min intervals, while the temperature was kept at 5-10 °C. After the addition of the sulfuric acid, the vigorous stirring was continued for 5 h, allowing the temperature to rise up gradually to 20-25 °C. The solution was cooled again (under ice bath) and neutralized with 50% sodium hydroxide solution under stirring. The addition was made slowly to avoid heating. A small amount of sodium hydrogen carbonate was added to maintain the solution near neutrality. The salts were removed by filtration and the acetone solution was concentrated under reduced pressure. The DX was extracted in *n*-hexane and crystalized after evaporation of *n*-hexane.

Nitrogen physisorption was carried out at 77 K on a Micromeritics ASAP 2420 apparatus. Prior to analysis, the samples were pretreated at 573 K under vacuum for 15 h. Coked samples were outgassed at 423 K for 1 h to avoid coke elimination. The micropore volumes (V_{micro}) were calculated using the *t*-plot method. The pore size distributions were determined using the density functional theory (DFT) model applied on the adsorption branch. The total pore volume was calculated at p/p_0 = 0.9. The mesopore volume (V_{meso}) was determined by the difference between the total pore volume and the micropore volume.

X-ray Diffraction (XRD) was performed using a Rigaku Ultima IV diffractometer (Cu $_{K\alpha}$ λ =0.1542 nm) at a scanning rate of 0.02^{o} s^{-1} in 2 θ ranges from 5 to 80^{o}. A fixed power source was used (40 kV, 20 mA).

Fourier transform Infrared spectra (FT-IR) of pyridine adsorbed samples were recorded on a Nicolet Magna 550-FT-IR spectrometer with a 2 cm^{-1} optical resolution. The zeolites were first pressed into self-supporting wafers (diameter: 1.6 cm, ≈ 20 mg) and pretreated from room temperature to 723 K (heating rate of 1.5 K min^{-1} for 5 h under a pressure of 1.33 10^{-4} Pa) in an IR cell connected to a vacuum line (samples with coke were outgassed at 363 K for 1 h and 423 K for 1 h and these conditions were used to minimize degradation and elimination of molecules presented in the coke, thus close to the coke formed *in situ* in the spent catalyst). Pyridine adsorption was carried out at 423 K. After establishing a pressure of 133 Pa at equilibrium, the cell was evacuated at 623 K to remove all physisorbed species. The amounts of pyridine adsorbed on the Brønsted and Lewis sites were determined by integrating the band areas at 1545 cm^{-1} and 1454 cm^{-1} respectively and using the following extinction coefficients measured at 293 K: ε_{1545} = 1.13 and ε_{1454} = 1.28 cm mol^{-1} [22].

The fluidize catalytic cracking unit used to convert the new bio-feed in this study is presented in Figure S1 [23]. The tests were carried out by using 10 mL of feed (pristine *n*-hexane and mixtures of DX up to 50 wt.% in *n*-hexane) injected over 1 min, and 20 g of the catalyst was used in the catalytic bed. Before the reaction, the catalyst was activated in a nitrogen atmosphere for 12 hours at 773 K. Nitrogen flow was calibrated at room temperature, and nitrogen flow at 200 ml min^{-1} (estimated at 773K using the state equation of ideal gas) was used to fluidize the catalyst. The reactor was operated in between 693-773 K considering the

height of the fluidized catalytic bed (Figure S2). Cat-A is a fresh commercial FCC catalyst supplied for this work by Petrobras, and was used with particle diameter 115 - 200 mesh equivalent to a particle size diameter of 0.125-0.08 mm respectively, but the composition is unknown. Also, a model FCC catalyst (Cat-B) with the following composition: USY, SiO_2, Al_2O_3 and Kaolin of 40, 20, 25 and 15 wt.% respectively was used [25]. For both catalysts, the catalytic results of DX and *n*-hexane mixtures were analysed and discussed by comparing with those observed in pristine *n*-hexane experiment.

The products from the cracking reactions were analyzed off-line. The liquid fraction was analyzed by both GCMS and CGFID. The GCMS system is an Agilent Technologies 7890A CG coupled to a 5975C MS in electron impact mode, an Agilent HP-5MS column was used and the oven temperature kept at 303 K for 7 min followed by a ramp to 443 K for 40 min, helium was used as carrier gas. At the inlet, a split ratio of 20:1, 14 psi pressure and 563 K was used. All samples were injected without dilution.

The *n*-hexane amount in the liquid fraction was quantified using the GCMS, *n*-hexadecane was used as an internal standard, the calibration profile is presented in Figure S3. This procedure was used to determine the n-hexane conversion. The liquid products were obtained by subtracting the liquid mass by the mass of non reacted *n*-hexane and according to the material balance adjusted as presented in Table S1. The proportions of aromatic and non-aromatic yields were determined by chromatography (the chromatographic factors used for aromatics were presented in Table S2 and for non-aromatics the same as that of *n*-hexane).

The amount of gas produced during the reaction was determined by the difference of water displaced during the reaction and the one in a pure nitrogen

flow (always quantified before reaction). The gas composition was determined by taking a sample of the gas inside the water Erlenmeyer as presented in Figure S1 and the analyses were repeated three times. Saturated salt water was used to prevent gas solubilisation. The gas composition (H2, CO, CO2 methane and hydrocarbon up to C4) was analysed using an Agilent Technologies MicroGC 490.

The amount of coke in the spent catalysts was determined through thermogravimetric analysis (Netzsch TG-IRIS). The samples were heated from 308 to 523 K at a rate of 10 °C min^{-1} under N_2 atmosphere. The temperature was kept at 523 K for 30 min, after which the atmosphere was changed to synthetic air (20.9% O_2 in N_2) and the temperature increased to 973 K at a rate 10 K min^{-1} and then maintained at 973 K for 30 min. The amount of coke in the catalyst corresponded to the weight loss at temperatures higher than 523 K and the coke yield was estimated comparing this value (considering the amount of catalyst in each reaction) to the total feed introduced into the reactor.

The chemical composition of coke was determined using the established methodology detailed in ref [26]. In order to release the molecules trapped in the zeolite pores, the zeolite framework was mineralized at room temperature with a 51% aqueous hydrofluoric acid (HF) solution. The coke molecules soluble in methylene chloride were subsequently analyzed by GC-MS (Thermo Electron DSQ with a DB5ms column). To determine the relative amount of gas and liquid products and coke, the above mentioned amounts determined were summed up and considered as 100%

198

199 **3 – Results and Discussion**

200

201 ***Catalyst characterization***

202 The textural and the acidic properties, of the commercial (Cat-A) and a
203 simplified FCC catalyst [24] (Cat-B) are reported in Table 1. Both catalysts present
204 very similar silica and alumina composition, and their diffraction patterns feature
205 characteristic peaks corresponding to FAU zeolite and kaolinite (12 and 25° 2θ)
206 diffraction planes (Figure S4).

207 The nitrogen adsorption and desorption isotherms at 77 K, Figure 1, of
208 Cat-A and Cat-B exhibit the typical shape expected for microporous materials
209 (type I isotherm), with an important nitrogen uptake at low relative pressure (<
210 0.15) followed by a plateau (0.15-0.90). At relative pressures close to saturation,
211 the isotherms feature an upward turn ascribable to nitrogen condensation within
212 secondary porosity due to the previous steaming of the Y zeolite to achieve USY.
213 Isotherms of both catalysts feature a H4 hysteresis loop at a relative pressure close
214 to 0.45, which is typical of steamed Y zeolite and indicates the presence of some
215 constricted and occulted mesopores in which desorption occurs through
216 cavitataion. The micropore volumes were calculated by Harkins-Jura *t*-plot and
217 amount to 0.13 $cm^3 g^{-1}$ for both catalysts. Considering that a typical FAU structure
218 features ~ 0.3 $cm^3 g^{-1}$ of microporous volume, it is possible to estimate that Cat-A
219 and Cat-B are composed of approximately 40 wt.% of the crystalline zeolite phase.
220 Hence, the commercial and simplified FCC catalysts feature similar textural
221 properties.

222

Table 1: Selected textural and acidic properties of Cat-A and Cat-B.

	SiO_2	Al_2O_3	V_{micro} [a]	V_{meso} [b]	$[PyH^+]_{150°C}$ [c]	$[PyL]_{150°C}$ [d]
	wt.%	wt.%	$cm^3\ g_{cat}^{-1}$	$cm^3\ g_{cat}^{-1}$	µmol g_{cat}^{-1}	µmol g_{cat}^{-1}
Cat-A	58.7	41.3	0.13	0.07	440	87
Cat-B	58.0	42.0	0.13	0.08	506	86

a: micropore volume determined by Harkins Jura *t*-plot; b: $V_{meso} = V_{total} - V_{micro}$ (V_{total}: determined from the adsorbed volume at $p/p_0=0.9$), c and d: concentrations of Brønsted ([PyH^+]) and Lewis ([PyL]) sites able to retain pyridine at 423 K.

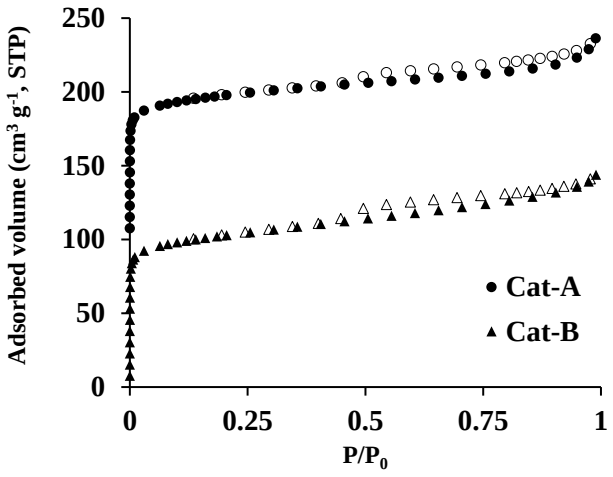

Figure 1. N_2 adsorption and desorption isotherms at 77 K of commercial (Cat-A) and simplified FCC catalysts (Cat-B). For a better visibility the isotherm of Cat-A was shifted by + 100 $cm^3\ g^{-1}$ along the Y axis.

FTIR spectroscopy was used to gather insights on the hydroxyl groups located on the catalyst surface. The IR spectra of Cat-A and Cat-B are presented in Figure 2. The $\nu_{(OH)}$ region shows two narrow and intense bands centered at 3696 and 3623 cm^{-1}, which can be ascribed to kaolinite with an ordered structure.[27] A band of less intensity at 3743 cm^{-1} can be assigned to isolated external silanols, and two bands at 3660-3640 cm^{-1} and 3537-3544 cm^{-1} can be related to bridging OH in supercages and hexagonal prisms, respectively (Figure 2). For FAU, all bridging OH groups, even those within the sodalite cages, interact with pyridine. A small portion of silanol is strong enough to retain pyridine. On the commercial catalyst (Cat-A), the employed binder features no acidic properties whereas on the simplified FCC catalyst (Cat-B), some OH of the kaolinite are able to interact with the organic base (Figure S4). The concentration of the Brønsted acid sites (BAS), is slightly lower on Cat-A (440 µmol g^{-1}) than on Cat-B (506 µmol g^{-1}). The concentrations of Lewis acid sites are similar on both catalysts (ca 86-87 µmol g^{-1}). Thus, Cat-B should be more active in cracking reactions compared to Cat-A. It is difficult to deduce the framework Si/Al ratio, as the amount of residual Na and other factors may lead to a misleading estimation.

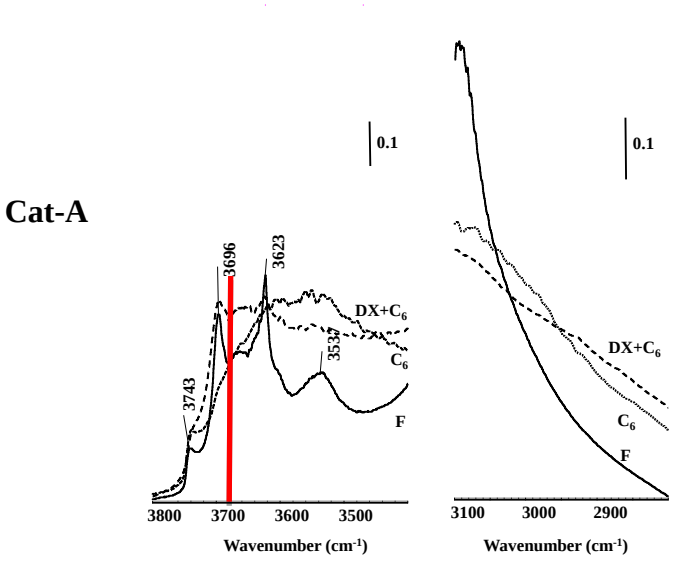

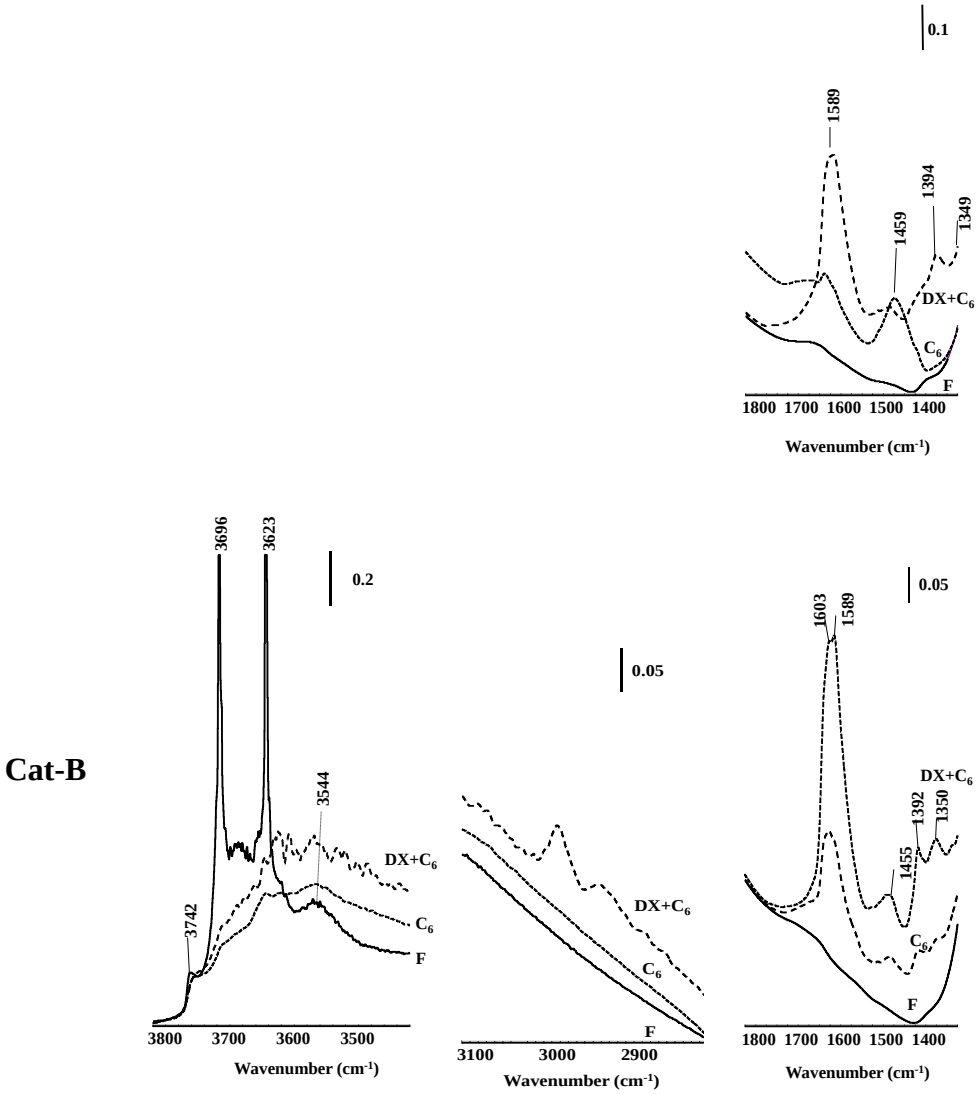

255

256 **Figure 2.** Evolution of bands in regions 3800-3400 cm^{-1}, 3100- 2700 cm^{-1} and

257 1800-1300 cm^{-1} on commercial (Cat-A) and simplified (Cat-B) FCC catalysts. F:

258 fresh, DX+*n*-C_6 and *n*-C_6: spent catalysts.

259

260

261

262

Product distribution and Material balance.

The material balance was checked by adding the masses of coke, liquid, and gas fractions produced during the reaction with the mass of the feed. All tests showed material balance around 100% (a range of 96-112 was observed) as presented in Table 2 and the error in the individual fractions vary approximately 10% (Table S3). For each test, three samples of the spent catalyst were analysed to determine the amount of coke formed, and no differences were observed.

Table 2. Products of transformation of DX and *n*-hexane mixtures: gas, liquid and coke in wt.% in relation to feed and coke amount on the spent catalyst in wt.% of the catalyst.

	Feed (g)	DX%	Gas	Liquid	Coke	Total	Coke% in cat.
Cat-A	6.55	0 (*n*-C_6)	25	75	11	111	3.4
	6.78	10	20	76	16	112	5.2
	7.29	30	23	63	16	102	5.9
	7.79	50	26	49	22	97	8.0
Cat-B	6.55	0 (*n*-C_6)	42	43	11	96	3.4
	7.29	30	39	39	15	96	5.3
Cat-B-DH	6.55	0 (*n*-C_6)	14	79	1	94	0.4
	7.29	30	9	81	8	98	2.8

Liquid fraction. The liquid phase was the main fraction obtained by converting pure *n*-hexane and *n*-hexane/DX mixtures in the presence of Cat-A. In contrast,

Cat-B favours the gas fraction and both gas and liquid fractions showed comparable values. Higher gas fraction is related to higher catalytic activity as expected based on the catalysts properties presented in Table 1. With the introduction of 10% of DX in the presence of Cat-A, no effect was observed in the liquid yield and the gas yield slightly decreased. Further increase in DX concentration to 30% slightly reduced liquid yield. Merely for the 50wt.% DX mixture a significant decrease in the liquid yield and increase in the coke yield occurred. The conversion of 30% of DX and *n*-hexane in the presence of Cat-B (that is more active than Cat-A) showed minor differences in both gas and liquid yields when compared with pristine *n*-hexane. The Cat-B-DH deactivated showed 50% reduction in coke yield, lower gas and higher liquid compared to the fresh Cat-B. By comparing these results it is clear that the catalyst controls the product yield distribution and suggests that further improvement in ketal sugar-derivative conversion is expected by diligent catalyst design. The FCC catalyst plays a central role in hydrocarbon conversion [25, 26] and likewise for the DX conversion.

The liquid fraction is separated into six main classes as presented in Table 3. Detailed quantitative results of selectivity are presented in Tables-S4 to -S7 and an example of a chromatogram is presented in Figure S5. The products that were identified were categorised in their respective classes. A very small amount of the products that could not be assigned was included in the non-identified product fraction. Practically no oxygenated compounds were identified in the liquid fraction in any of the tests of fresh catalyst summarized in Table 2. The 50% DX in *n*-hexane mixture showed the highest number of non-identified products. Heavy compounds were barely observed in all tests in the presence of Cat-A and not

304 detected in the presence of Cat-B. For Cat-B-DH large amounts of acetone were
305 produced.
306
307
308

Table 3: Liquid products obtained from the conversion of pure *n*-hexane and mixtures with 10, 30 and 50 wt.% DX. Products (in wt.% of the liquid phase) in the liquid phase are separated by class S_{Ar} (aromatic compounds), S_{ole} (olefin containing five or more carbons), S_{sat} (paraffins containing five or more carbons), S_{light} (compounds containing four or less carbons), non-identified (products not identified and oxygenates), Heavy (poly-aromatic), and $S_{non\ Ar}$ (S_{ole} + S_{sat}).

Catalyst	Cat-A				Cat-B		Cat-B-DH	
Feed	*n*-C_6	10%	30%	50%	*n*-C_6	30%	*n*-C_6	30%
S_{Ar}%	9	24	42	56	18	50	4.3	23.9
S_{ole}%	17	11	6	4	18	6	-	-
S_{sat}%	25	22	15	9	27	13	-	-
S_{light} ($C4^-$) %	49	40	32	17	34	26	96	31
Non-identified %	0	1	3	8	2	2	0	4
Heavy %	0	2	3	5	1	2	0	2
acetone	0	0	0	0	0	0	0	38
$S_{non\ Ar}$%	42	33	20	14	45	20	-	-
S_{ole}/S_{sat} ratio %	0.69	0.52	0.40	0.46	0.68	0.49	-	-
n-hexane conv. %	68	65	54	55	70	63	55.7	36.4
Est. $S_{non\ Ar}$ %*	-	36	26	18	-	17	-	-
Est. S_{light}%*	-	42	30	20	-	12	-	25

* Both Est. $S_{non\ Ar}$ and Est. S_{light}% were estimated assuming that these classes were produced exclusively by n-hexane (the estimate was obtained removing non converted *n*-hexane in the liquid phase, multiplied by the selectivity of its transformation in pristine form).

DX was fully converted in all tests and *n*-hexane conversion slightly decreased in DX mixtures in the presence of fresh catalysts. Also the mixture of 30wt% DX in *n*-hexane showed lower conversion decrease in the presence of Cat-B compared to Cat-A.

The aromatic compounds are mainly alkyl-mono-aromatics such as toluene, xylene up to three and four alkyl carbons (detail distribution is presented in Tables-S4 to S7). The conversion of *n*-hexane in the presence of Cat-A and Cat-B afforded 9% and 18% of aromatics, respectively. It can be rationalized that the superior acidity of Cat-B favours sequential reactions to aromatic compounds. Likewise, Cat-B shows excessive cracking to light hydrocarbons increasing the gas yield (as presented in Table 2).

As a result of the introduction of 10% of DX in *n*-hexane, the aromatic content remarkably increased (3-fold) compared to pristine *n*-hexane. The aromatic content increased almost linearly with the DX concentration (Figure 3-a). Cat-B showed higher contents of aromatic compounds for both pristine *n*-hexane and 30% DX in *n*-hexane in comparison to Cat-A. The non-aromatic fraction (Figure 3-a) is composed of olefins and paraffins. Previous results, using labeled DX in xylofuranose carbons, showed the absence of labeled carbon in paraffins and olefins. Thus these compounds were almost exclusively derived from *n*-hexane conversion[15]. Yet, the contribution of isopropylidene groups cannot be ruled out.

To support the consideration of the origin of the non-aromatics, values for the non-aromatic fraction, presented in Table 3, were estimated based on the following two assumptions: 1 – it is exclusively produced by *n*-hexane; 2 – the

yield was determined (as explained in the experimental section) and the selectivity of *n*-hexane conversion was not affected by the presence of DX. The estimated contribution of *n*-hexane and the measured values are similar for both catalysts, which supports the conclusion that these products are mainly related to the *n*-hexane conversion as previously noted[14].

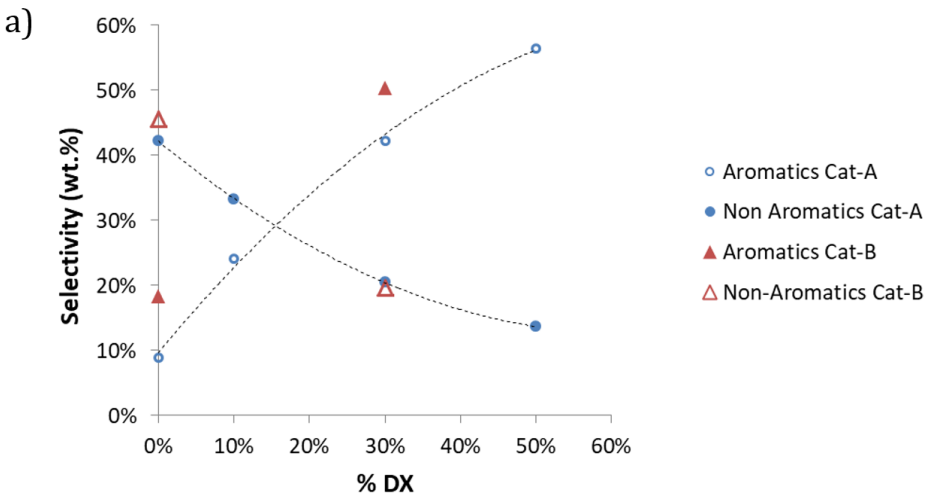

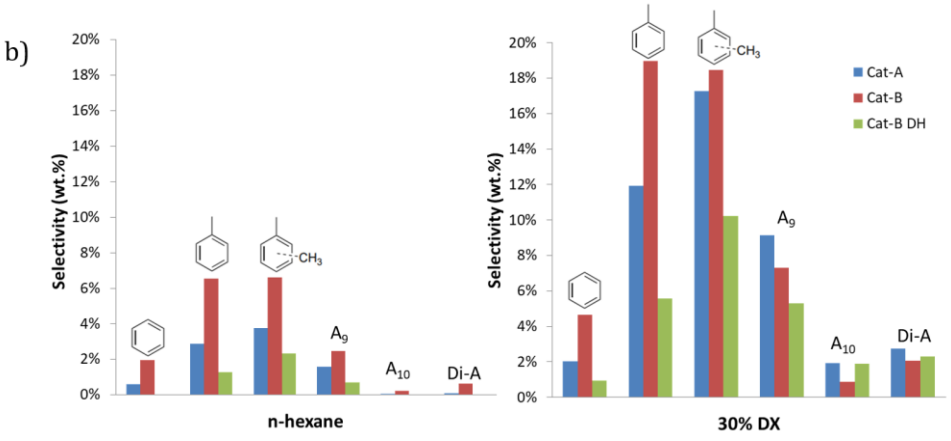

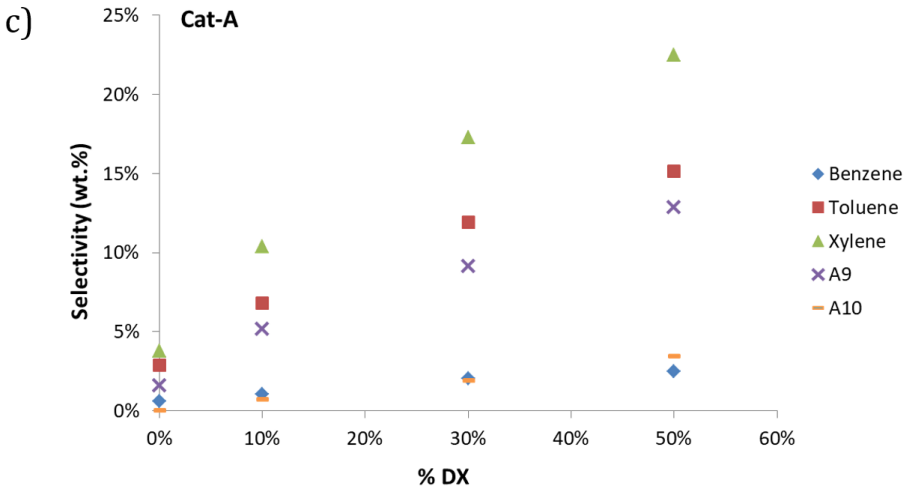

Figure 3: (a) selectivity of total aromatics and non-aromatics as wt.% of the liquid products for converted mixtures of DX in *n*-hexane and pristine *n*-hexane in the presence of Cat-A and Cat-B. **(b)** Aromatic selectivity as wt.% of each products of the total liquid products obtained by pristine *n*-hexane and mixture with 30% DX in the presence of Cat-A, Cat-B and Cat-B-DH. **(c)** Aromatic selectivity as wt.% of each product type of the total liquid products in function of DX concentration in the presence of Cat-A.

The distribution of aromatic compounds obtained in *n*-hexane and 30wt.% DX in *n*-hexane are presented in figure 3-b. This distribution was slightly affected by the type of catalyst, for instance toluene selectivity was favoured in the presence of Cat-B, while mono aromatics containing C9 were favoured in the presence of Cat-A. For the same catalyst (Cat-A), an increase of DX in the mixture increased the aromatics but the relative amount of benzene, toluene and xylenes was maintained, while alkyl-aromatic containing nine carbons and more were slightly affected as presented in figure 3-C. This complex variation of the catalysts

on the type of aromatic cannot be clarified under high conversion regime and will be further explored in later works.

The yields (in wt.% of total feed) of coke, aromatic, non-aromatic and gas in the presence of Cat-A are presented in figure 4-a. Mono-aromatic yield continually increased with an increase of DX concentration while non-aromatic and gas yields decreased. Particularly, the higher decrease in liquid fraction observed for the 50%DX mixture was compensated by the higher aromatic selectivity. Gas yield did not follow a tendency and coke yield increased which is discussed in the section devoted to coke formation. The conversion in the presence of Cat-B showed high yield of gas. In contrast, gas and coke yields remarkably decreased in the presence of Cat-B-DH. Both Cat-B and Cat-B-DH showed similar aromatic yield. The remarkable effect of the catalyst on the product distribution constitutes a major advance and suggest that advanced catalyst development is a promising solution to further increase the aromatic yields.

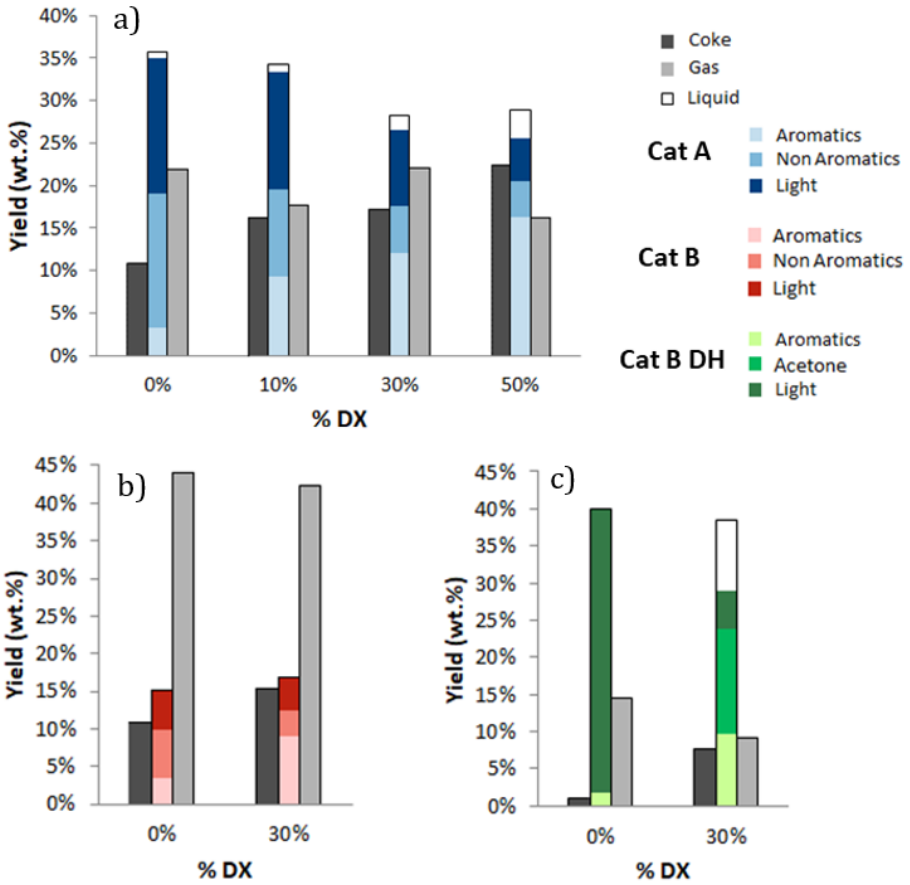

Figure 4: Yield (wt.% of total products) of coke, aromatics, non-aromatics and gas in the presence of Cat-A (a), Cat-B (b) and Cat-B-DH (c).

The remaining products in the liquid phase are solely related to light compounds (S_{light}). It is worth to mentionthat it is difficult to precisely determine the amount of light products as they are partially distributed in both the liquid and gas phase. The light products can be further solubilized in the aqueous NaCl phase, in the apparatus for the gas displacement measurement. An estimated contribution of *n*-hexane to the formation of light products, similar to the one made for the non-aromatics, resulted in very similar values to those measured for each test in the presence of Cat-A, but different values in the presence of Cat-B.

The olefin/saturated ratio (S_{ole}/S_{sat}) presented in Table 3 decreased in the mixture of 10%DX in the presence of Cat-A, and further reduced in the 30%

DX/*n*-hexane in the presence of Cat-A compared to pristine *n*-hexane. Further increase to 50%DX did not lead to changes in conversion, yet S_{ole}/S_{sat} ratio increased. In the presence of Cat-B this ratio also reduced in the presence of DX compared with pristine *n*-hexane. This complex variation of (S_{ole}/S_{sat}) may not only be due to the influences of DX on the conversion of *n*-hexane but further on the reaction path of *n*-hexane. This will be further explored by refining the product analysis in later works.

Gas fraction. The gas composition contains hydrocarbons of up to four carbons, hydrogen, CO and CO_2 as presented in Table 4. The CO and CO_2 ratio is similar for all tests. CO_2 and CO could be dissolved in the apparatus for the gas measurement and the uncertainties in the experimental setup limits specific conclusions on the evolution of deoxygenation from DX. Likewise, material balance regarding oxygen cannot be provided so far. Similarly, the experimental set up (that does not avoid entirely the condensation of light hydrocarbons at 258 K) may cause uncertainties in the quantification of heavier compounds in the gas phase. Gas phase products of pristine *n*-hexane are comparable to results observed in the literature [27, 28], mainly C_3 and C_4 products are formed followed by ethylene and ethane and a small amount of methane and hydrogen. The last two are related to the protolysis of the σ carbon(primary)-carbon and carbon-hydrogen bonds of *n*-hexane respectively by the zeolite acid sites [29]. Methane selectivity progressively increased by increasing the DX concentration in the presence of Cat-A and was not affected in the presence of Cat-B. Both ethylene and propylene also slightly increased, in contrast, both propane and butane concentrations decreased with increasing DX concentration.

Among all products, the most notable is that the propane selectivity reduced in the presence of DX. The combined effect on olefin and propane resulted in a remarkable increase in the ratio of olefin/paraffin from pristine *n*-hexane to 50%DX/*n*-hexane mixture as presented in table 4. To reduce the influence of *n*-hexane conversion on propane selectivity only tests with similar conversion were compared in the following discussion. The n-hexane conversion slightly decreased comparing pure *n*-hexane with 10%DX, yet propane selectivity decreased from 61 to 53. The mixtures of 30 and 50% DX in *n*-hexane showed the same *n*-hexane conversion and even a higher decreased was observed in propane selectivity. Cat-B showed similar results. As propane is mainly produced by *n*-hexane, the obtained results indicate that DX affects the *n*-hexane conversion path.

Table 4: Gas composition of DX and *n*-hexane experiments for Cat-A and Cat-B.

		Gas (%molar)										
		H_2	CH_4	C_2H_4	C_2H_6	C_3H_8	C_3H_6	C_4H_{10}	C_4H_8	CO	CO_2	$\frac{olef.}{Sat.}$
Cat A	*n*-hexane	1	5	5	2	61	9	16	1	0	0	0.189
	10%DX	1	7	5	3	53	8	17	1	2	3	0.192
	30%DX	1	9	7	2	41	12	14	1	7	6	0.345
	50%DX	1	20	10	2	25	10	11	1	10	9	0.556
Cat B	*n*-hexane	2	8	5	3	65	9	7	2	0	0	0.213
	30%DX	2	8	5	3	46	9	15	1	9	8	0.233

Coke fraction. As shown in Figure 4c and Table 2, the coke yield ranges from 10 to 20% for fresh catalysts and reduces considerably to less than 10% for the deactivated catalyst. Coke yield increased with the increase in DX in the feed

mixture. However, the increase in coke on catalysts for a 30%DX mixture compared to pure *n*-hexane was only 2.5 wt% or less. A commercial FCC unit operates in the temperature range of 773-808 K and the reaction occurs within short contact times, *i.e.*, 3 to 7 seconds [30, 31]. In general, a spent FCC catalyst exhibits 1wt.% of coke on the catalyst. This represents an amount of 5-10 (wt.%) of the feed being converted into coke for a catalyst/feed ratio (in wt.) in the range of 5 to 10. In our experiments, the catalyst/feed ratio was three times lower and the contact time was 60 seconds. These condition are regularly applied in laboratory fluidized units[32, 33] and responsible for the large amount of coke formation when compared to real FCC units. Hence, the coke yield for fresh catalyst in laboratory units should be compared only with test effectuated under same conditions.

Preliminary results of deactivation were obtained in the Cat-B-DH that indicated a reduction of 50% of the coke yield. However, high amount of acetone was observed. Hence, the deactivation treatment and test condition should be improved.

On the commercial and synthesized FCC catalyst, the coke content increases proportionally with the weight percent of DX in *n*-hexane (Figure 4a). Indeed, many studies have shown that the co-feeding strategy of oxygenates such as phenol[34, 35], *m*-cresol[36] and bio-oil[37]with hydrocarbons increases the coke yield, which is ascribable to the strong adsorption of oxygenated molecules on zeolite acid sites. The FCC units are designed to handle coke on the catalyst to a certain extent. Yet excessive coke formation, as observed during the processing of oxygenated feeds[38], could limit the amount or even hinder the co-processing of renewable feeds. The relative small amount of coke using fresh catalyst and the

decrease using deactivated catalyst to convert a model feed containing a high concentration of DX is a very encouraging result.

Infrared spectra of spent catalysts obtained through different feed composition (*n*-C_6 and 30% DX/*n*-C_{-6}) are presented in Figure 2. The bands of carbonaceous compounds deposited on zeolites were observed in two domains. In the region of 2700-3100 cm^{-1} corresponding to the CH stretching modes of aromatic and paraffinic groups, and 1300-1700 cm^{-1} ascribable to CC stretching modes of unsaturated (olefin, polyenyl, aromatic and polyaromatic) groups and CH bending of paraffinic groups (Figure 2). The band at 1459 cm^{-1} can be attributed to coke precursor molecules with a limited number of aromatic rings (N_{AR}) to 2 and 3 [39]. The bands at 1603, 1589, 1392 and 1350 cm^{-1} are related to polyaromatic coke (N_{AR} ≥4)[40]. On all spent catalysts, the absence of CH stretching modes, as their low intensity for the spent Cat-B after *n*-C_6 conversion, indicates a low degree of alkylation of the coke molecules. In the presence of DX in the feed, the intensity of the bands of the polyaromatic compounds were more intense, which indicates a coke formation with higher complexity. Yet, the increased intensity may partly be due to higher content (Table 2, Figure 2).

The composition of coke trapped within the zeolite pores, *i.e.* internal coke, was determined by mineralizing the zeolite matrix and subsequently analyzing the organic residue by liquid-liquid extraction with CH_2Cl_2. A minor fraction of coke molecules was insoluble in methylene chloride. Even at low coke content, the recovered coke molecules consist mainly of polyaromatic compounds with an N_{AR} from at least 4 (pyrene, M_w: 202 g mol^{-1}, d: 1.27) and up to 7 (coronene, M_w: 300 g mol^{-1}, d: 1.37). The estimated average molar mass and density of the coke trapped in the micropores is 250 g mol^{-1} and 1.3, respectively. The presence of DX

492 in the feed, even at high concentrations, has no impact on the chemical
493 composition of coke. Thus, no evidence of oxygenated trapped products was
494 found. Yet, several studies pointed out that two pathways of coke formation occur
495 in the co-feeding of hydrocarbons and oxygenates. The oxygenate pathway,
496 forming polyphenols residues with more aliphatic and oxygenated nature[41,
497 42]from aldol condensation[43] and the hydrocarbon pathway, forming
498 polycondensed aromatic structures. It is surprising that applying a temperature
499 close to real FCC the test favours the hydrocarbons pathways in the coke
500 composition even with of high content of oxygenates in the feed[37, 44].
501 Apparently, the coke formed by DX cracking differs to the one formed by catalytic
502 cracking of fast pyrolysis bio-oil that is partially oxidized [45] .

503 The decrease of the Brønsted acid sites and of the micropore volume is
504 proportional to the coke content (Figure 5b and Figure 5d). Taking the above
505 determined average molar mass for the coke molecules trapped inside the
506 micropores into consideration, the number of coke molecules corresponds to the
507 amount of the deactivated Brønsted acid sites **(**Figure 5a). Moreover, the real
508 (calculated from estimated density) and apparent (measured by N_2 physisorption)
509 micropore volumes occupied by coke molecules (Figure 5b) are identical,
510 suggesting that the majority of the coke is trapped within the micropores and not
511 on the external surface. Indeed the silanol groups located on the external (or
512 mesopore-) surface, were not impacted by coke deposition (Figure 2). The
513 decrease of the OH groups (3696 and 3623 cm^{-1}) of the binder can occur at high
514 temperature during the cracking reaction and yield to the formation of Lewis acid
515 sites (LAS). After *n*-hexane cracking, their concentration is twice to three times
516 higher than that of the fresh catalysts (Figure 3d). Their concentration decreases

with the coke content as function of the DX concentration. This decrease probably concerns only the LAS located in the zeolite crystal, which accessibility to pyridine decreases with increasing coke content in the micropores. DX co-feeding increased coke formation, however, without affecting its toxicity and hence the coking mode (*i.e.* poisoning).

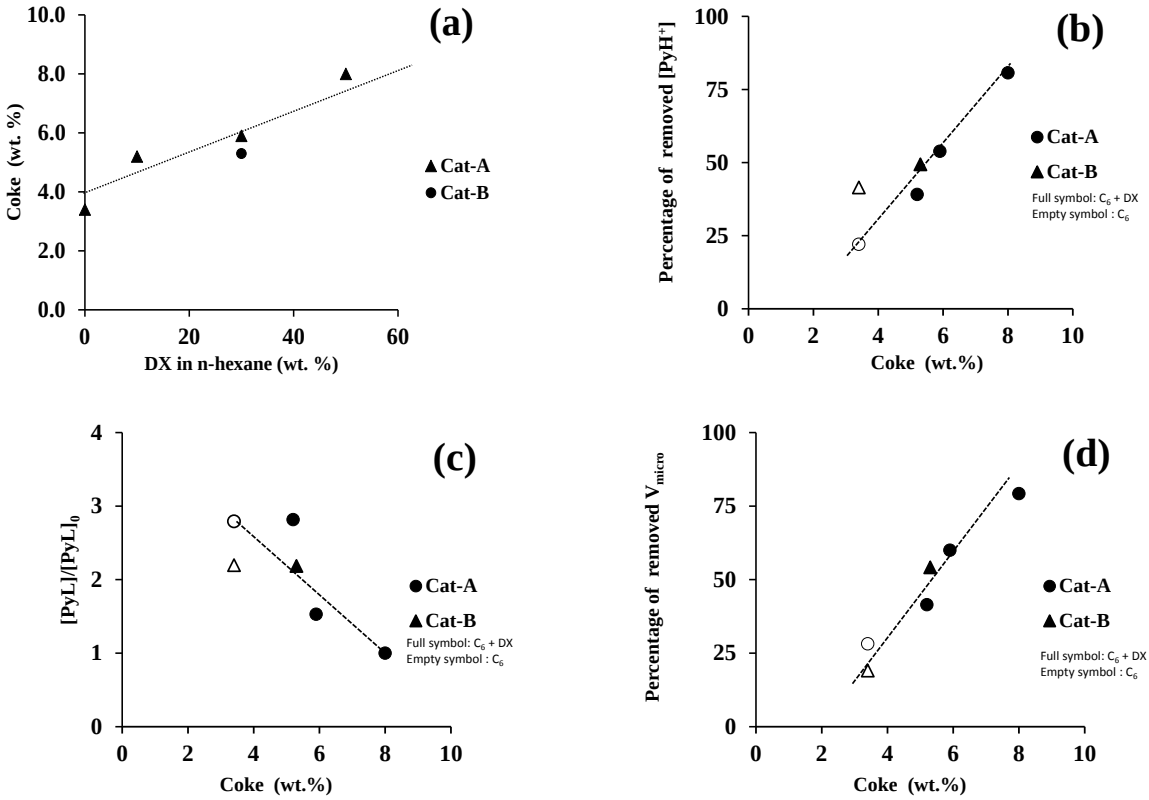

Figure 5. Coke content as a function of DX concentration for *n*-hexane cracking (**a**), percentage of removed Brønsted acid sites, (**b**) proportion of Lewis acid sites (**c**) and microporous volume (**d**) on the spent catalyst as a function of the coke content.

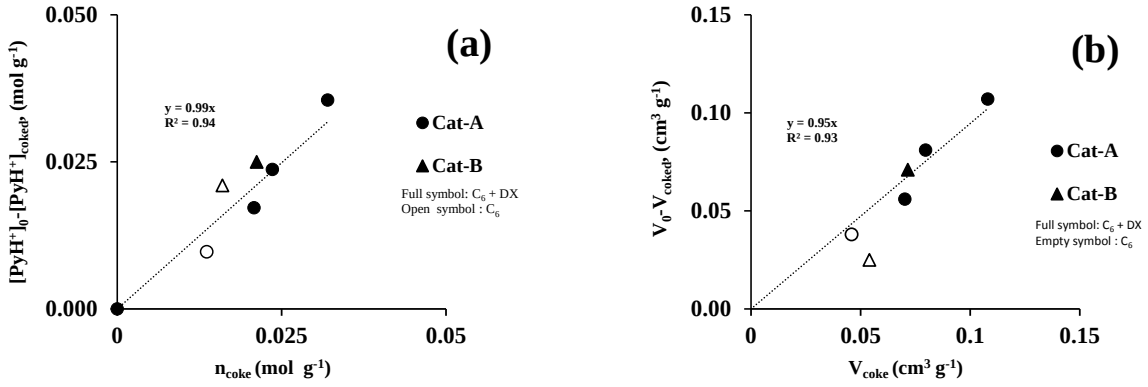

528 **Figure 6.** Coking mode: (a) number of deactivated Brønsted acid sites as a
529 function of the number of coke molecules; (b) apparent volume occupied by coke
530 molecules as a function occupied pore volume deduced by nitrogen physisorption.

531

532 **Consideration on mutual DX and *n*-hexane interactions**

533 Hydrocarbon chemistry over acid catalysts is governed by bimolecular
534 reactions [26, 28, 46] and particularly by hydrogen transfer reactions[32]. For
535 instance, hydrogen transfer reaction between olefins and naphthenes leads to the
536 formation of more refractory paraffins [47, 48]. Primarily, hydrocarbon is
537 activated by protolytic reaction on both σ C-H and C-C bonds,[29] [23]. Sequentially
538 to the carbenium ion several bimolecular reactions could occur, particularly at
539 moderate conversion the interconversion of olefins[54] and products (as function of
540 the zeolite structure) [55] undergoes sequential reactions until formation of
541 aromatics, poly-aromatics and coke[37]. *n*-Hexane reaction on acid catalysts such as
542 Y and ZSM-5 affords products containing mainly 3 and 2-4 carbons related to both
543 mono- and bi-molecular reactions [31]. The olefin to paraffin ratio in the gas phase is
544 a typical index for bimolecular hydrogen transfer reaction. The present results
545 showed that with similar *n*-hexane conversion, gas phase olefin/saturated ratio

546 increased and propane selectivity decreased by increaseing the DX concentration
547 in the feed mixture.

548 Despite of large decrease in Brønsted acid sites and micro porous volume
549 due to coke deposit, DX was entirely converted using both fresh and deactivate
550 catalysts and *n*-hexane conversion only slightly decreased in the mixture feed
551 compared to that observed in *n*-hexane. The higher DX reactivity is expected base
552 on higher basicity due to non-bonded electron pair of its oxygen atoms. Indeed *n*-
553 hexane is poorly reactive as expected by the lower σ C-C and C-H basicity. Yet it
554 is worth to mention that in the mixture of 30%DX/*n*-hexane the *n*-hexane
555 conversion decreased only 20 and 10% of in the presence of Cat-A and –B,
556 respectively. Hence, it appears that DX (a more active molecule) could be
557 primarily activated, then, *n*-hexane (a less active molecule) could participate in the
558 catalytic-turnover mainly initiated by DX.

559 The mutual interaction between *n*-hexane and DX (and their products)
560 could manifest beyond a mere competition of acid sites during co-processing. The
561 competition by acid sites was proposed to justify the reduction of gasoil
562 conversion during the co-processing with pyrolysis bio-oils. We will continue
563 investigating this hypothesis through designed experiments with feed variations,
564 detail analysis of activity and overall product distribution.

565 4 – Outlook

566 From a fundamental point of view, the distribution of reaction products, the
567 amount and properties of the coke and other observations from the DX and *n*-
568 hexane reactions indicate possible mutual influences of DX on *n*-hexane and vice
569 versa. Further studies are required to confirm whether bi-molecular reactions, such
570 as hydrogen transfer, between hydrocarbons and most probably oxygenated

intermediates occur. The in the presence of hydrocarbons enhanced deoxygenation could be related to the decrease of coke formation in the tests using bio-crude and gasoil mixture as previously reported [14].

Comparing the results achieved through using various catalysts and deactivated catalysts indicated that the catalyst playes an mayor role in the co-process. This reinforces that ketal compounds are promising and could be selectively converted into fuel in the refinery by a proper choice of catalyst and process conditions.

Finally, this work proves that transforming second generation biomass into bio-crude composed by sugar ketal derivatives represents a sound strategy for bio-aromatic production for petrochemical application. However, it is important to point out that *n*-hexane is not a representative compound of gasoil for co-processing in FCC operation. It is remarkably less reactive compared to a typical industrial feed. It is expected, that by co-processing DX to a gasoil feed, a more important ratio of DX could be used without impacting gasoil conversion. The results of this extension work will soon be reported.

5 – Conclusion

A representative compound of a bio-crude composed of ketal-sugar derivative, the 1,2:3,5-di-O-isopropylidene-α-d-xylofuranose (DX), was converted in the presence of *n*-hexane in fluidized catalytic cracking (FCC) using typical FCC catalysts.

DX was fully converted and mainly into bio-aromatics of the gasoline range. Our results indicate that important amounts of DX can be co-fed to *n*-hexane. *n*-Hexane conversion during co-process was slightly decreased in the

presence of DX. The coke yield on catalysts was low even in the laboratory catalytic unit, which usually leads to higher coke formation compared to commercial units. The formed coke did not contain detectable amount of oxygenated residue. The result suggests that DX would afford lower coke yield when compare to other type of bio-feed used in FCC in the same conditions.

5-Acknowledgment

Joana Pinto thanks CAPES for the scholarship, Marcelo Pereira thanks Petrobras for the catalyst, CNPq, and Faperj. We appreciate the technical assistance of both Hugo Rodrigues and Dr. Praveen Lawrence.

The authors acknowledge financial support from the European Union (ERDF) and "Région Nouvelle Aquitaine".

6- References

[1] E.S. Domalski, Selected values of heats of combustion and heats of formation of organic compounds containing the elements C,H,N,O,P, and S, J.Phys Chem., 1, number 2 (1972) 221-277.

[2] G.W. Huber, R.D. Cortright, J.A. Dumesic, Renewable Alkanes by Aqueous-Phase Reforming of Biomass-Derived Oxygenates, angew Chem Int Ed, 43 (2004) 1549 –1551.

[3] J.S. Luterbacher, Jacqueline M. Rand, David Martin Alonso, Jeehoon Han, J. Tyler Youngquist, Christos T. Maravelias, Brian F. Pfleger, James A. Dumesic, Nonenzymatic Sugar Production from Biomass Using Biomass-Derived g-Valerolactone, Science, 343 (2014) 277-280.

621 [4] G.W. Huber, S. Iborra, A. Corma, Synthesis of Transportation Fuels from
622 Biomass: Chemistry, Catalysts and Engineering, Chemical Reviews, 106
623 (2006) 4044-4098.
624 [5] G. Jiménez-García, R. Maya-Yescas, Differences between Fisher–Tropsch
625 synthesis of either gasoline or diesel based on changes of entropy and free
626 energy, Fuel, 149 (2015) 184-190.
627 [6] J.D. Adjaye, N.N.Bakhshi, Production of Hydrocarbons by catalytic
628 upgrading of a fast pyrolysis bio-oil. Part I: Conversion over various catalysts,
629 Fuel Processing Technology, 45 (1995) 161-183.
630 [7] M.C. Samolada, W. Baldauf, I.A. Vasalos, Production of a bio-gasoline by
631 upgrading biomass flash pyrolysis liquids via hydrogen processing and
632 catalytic cracking, Fuel, 77 (1998) 1667-1675.
633 [8] M.S. Talmadge, R.M. Baldwin, M.J. Biddy, R.L. McCormick, G.T. Beckham,
634 G.A. Ferguson, S. Czernik, K.A. Magrini-Bair, T.D. Foust, P.D. Metelski, C.
635 Hetrick, M.R. Nimlos, A perspective on oxygenated species in the refinery
636 integration of pyrolysis oil, Green Chemistry, 16 (2014) 407-453.
637 [9] Z. Wang, T. He, J. Qin, J. Wu, J. Li, Z. Zi, G. Liu, J. Wu, L. Sun, Gasification of
638 biomass with oxygen-enriched air in a pilot scale two-stage gasifier, Fuel, 150
639 (2015) 386-393.
640 [10] R.H. Venderbosch, A.R. Ardiyanti, J. Wildschut, A. Oasmaa, H.J. Heeres,
641 Stabilization of biomass-derived pyrolysis oils, Journal of Chemical
642 Technology & Biotechnology, 85 (2010) 674-686.
643 [11] A.d.R. Pinho, M.B.B. de Almeida, F.L. Mendes, V.L. Ximenes, L.C.
644 Casavechia, Co-processing raw bio-oil and gasoil in an FCC Unit, Fuel
645 Processing Technology, 131 (2015) 159-166.

646 [12] S. Wang, Q. Cai, J. Chen, L. Zhang, L. Zhu, Z. Luo, Co-cracking of bio-oil
647 model compound mixtures and ethanol over different metal oxide-modified
648 HZSM-5 catalysts, Fuel, 160 (2015) 534-543.
649 [13] S. Wang, Q. Cai, X. Wang, L. Zhang, Y. Wang, Z. Luo, Biogasoline
650 Production from the Co-cracking of the Distilled Fraction of Bio-oil and
651 Ethanol, Energy & Fuels, 28 (2013) 115-122.
652 [14] N. Batalha, A.V.d. Silva, M.O.d. Souza, B.M.C.d. Costa, E.S. Gomes, T.C. Silva,
653 T.G. Barros, M.L.A. Gonçalves, E.B. Caramão, L.R.M.d. Santos, M.B.B. Almeida,
654 R.O.M.A.d. Souza, Y.L. Lam, N.M.F. Carvalho, L.S.M. Miranda, M.M. Pereira,
655 Gasoline from Biomass through Refinery-Friendly Carbohydrate-Based Bio-
656 Oil Produced by Ketalization, CHEMSUSCHEM, 7 (2014) 1627–1636.
657 [15] N. Batalha, J. Pinto, H. Ferreira, D.C. Baptista, L.S.M. Miranda, M.M.
658 Pereira, Biohydrocarbons Production under Standard Refinery Conditions by
659 means of a Representative Ketal Compound of Biocrude, Energy Technology,
660 5 (2016) 428-441.
661 [16] R. Garrett, T.G. Barros, M.O. de Souza, B.M.C. da Costa, M.M. Pereira, L.S.M.
662 Miranda, Unveiling the chemical composition of sugar cane biocrudes by
663 liquid chromatography-tandem mass spectrometry, Energy & Fuels, 29
664 (2015) 8082-8087.
665 [17] Y.M. Questell-Santiago, R. Zambrano-Varela, M. Talebi Amiri, J.S.
666 Luterbacher, Carbohydrate stabilization extends the kinetic limits of chemical
667 polysaccharide depolymerization, Nature Chemistry, (2018).
668 [18] A.D.F. Ferreira, A.J. Maia, B. Guatiguaba, M.H. Herbst, P.T.L. Rocha, M.M.
669 Pereira, B. Louis, Nickel-doped small pore zeolite bifunctional catalysts: A way

to achieve high activity and yields into olefins, Catalysis Today, 226 (2014) 67-72.

[19] B.G. Anderson, R.R. Schumacher, R.v. Duren, A.P. Singh, R.A.v. Santen, An attempt to predict the optimum zeolite based catalyst forselective cracking of naphtha-range hydrocarbons to light olefins, Journal of Molecular Catalysis A: Chemical, 181 (2002) 291–301.

[20] A.J. Maia, B. Louis, Y.L. Lam, M.M. Pereira, Ni-ZSM-5 catalysts: Detailed characterization of metal sites for proper catalyst design, Journal of Catalysis, 269 (2010) 103-109.

[21] M. Guisnet, L. Pinard, Characterization of acid-base catalysts through model reaction, Catalysis Reviews, 60 (2018) 337-436.

[22] C. Miranda, J. Urresta, H. Cruchade, A. Tran, M. Benghalem, A. Astafan, P. Gaudin, T.J. Daou, A. Ramírez, Y. Pouilloux, A. Sachse, L. Pinard, Exploring the impact of zeolite porous voids in liquid phase reactions: The case of glycerol etherification by tert-butyl alcohol, Journal of Catalysis, 365 (2018) 249-260.

[23] J.F. Pinto, L.S.M. Miranda, P.M. Marcelo, Petroleum Refining and Oil Well Drilling. , in: K.F. Olson (Ed.) Problems, process and industry prospects, Nova Science Publishers, Nova York, 2017, pp. 314.

[24] F.V. Pinto, A.S. Escobar, B.G. de Oliveira, Y.L. Lam, H.S. Cerqueira, B. Louis, J.P. Tessonnier, D.S. Su, M.M. Pereira, The effect of alumina on FCC catalyst in the presence of nickel and vanadium, Applied Catalysis A: General, 388 (2010) 15-21.

[25] S.J. Miller, C.R. Hsieh, Octane Enhancement in Catalytic Cracking by Using High-Silica Zeolites, in: M.L. Occelli (Ed.) Fluid Catalytic Cracking II. Concepts in Catalyst Design-American Chemical Society, 1991, pp. 96-108.

695 [26] H. Abrevaya, Cracking of naphtha range alkanes and naphthenes over
696 zeolites, Studies in Surface Science and CAtalysis, 170 (2007) 1244-1251.
697 [27] T.F. Narbeser, H. Vinek, J.A. Lercher, Monomolecular Conversion of light
698 Alkanes over H-ZSM-5, Journal of Catalysis, 157 (1995) 388-395.
699 [28] A. Corma, A.V. Orchillés, Current views on the mechanism of catalytic
700 cracking, Microporous and Mesoporous Materials, 35-36 (2000) 21-30.
701 [29] B. Louis, M.M. Pereira, F.M. Santos, P.M. Esteves, J. Sommer, Alkane
702 activation over acidic zeolites: the first step, Chemistry, 16 (2010) 573-578.
703 [30] P. O'Connor, Catalytic Cracking: The Future of an Evolving Process, in:
704 M.L. Occelli (Ed.) Fluid Catalytic Cracking VII: Materials, Methods and Process
705 Innovations, Elsevier B.V.2007, pp. 227-250.
706 [31] E.T.C. Vogt, G.T. Whiting, A.D. Chowdhury, B.M. Weckhuysen, Zeolites and
707 Zeotypes for Oil and Gas Conversion, elsevier2015.
708 [32] A. Corma, L. Sauvanaud, FCC testing at bench scale: New units, new
709 processes, new feeds, Catalysis Today, 218-219 (2013) 107-114.
710 [33] J.C. Kayser, VERSATILE FLUIDIZED BED REACTOR, Kayser Technology,
711 Inc., Houston, Tex., United States 2000, pp. 13.
712 [34] I. Graça, J.D. Comparot, S. Laforge, P. Magnoux, J.M. Lopes, M.F. Ribeiro,
713 F.R. Ribeiro, Effect of phenol addition on the performances of H–Y zeolite
714 during methylcyclohexane transformation, Applied Catalysis A: General, 353
715 (2009) 123-129.
716 [35] I. Graça, A. Fernandes, J.M. Lopes, M.F. Ribeiro, S. Laforge, P. Magnoux, F.
717 Ramôa Ribeiro, Effect of phenol adsorption on HY zeolite for n-heptane
718 cracking: Comparison with methylcyclohexane, Applied Catalysis A: General,
719 385 (2010) 178-189.

720 [36] P. Sirous Rezaei, H. Shafaghat, W.M.A.W. Daud, Origin of catalyst
721 deactivation in atmospheric hydrogenolysis of m-cresol over Fe/HBeta, RSC
722 Advances, 5 (2015) 51278-51285.
723 [37] Á. Ibarra, E. Rodríguez, U. Sedran, J.M. Arandes, J. Bilbao, Synergy in the
724 Cracking of a Blend of Bio-oil and Vacuum Gasoil under Fluid Catalytic
725 Cracking Conditions, Industrial & Engineering Chemistry Research, 55 (2016)
726 1872-1880.
727 [38] M.M. Pereira, L. Benoit, Carbon dioxide, chemical valorization, and
728 mitigation in the refinery, in: S.L. Suib (Ed.) New and Future Developments in
729 Catalysis: Catalysis for remediation and environmental concerns,
730 Elsevier2013, pp. 535-562.
731 [39] H.S. Cerqueira, P. Ayrault, J. Datka, M. Guisnet, Influence of coke on the
732 acid properties of a USHY zeolite, micro and mesoporous material, 38 (2000)
733 197-205.
734 [40] N. Chaouati, A. Soualah, M. Chater, M. Tarighi, L. Pinard, Mechanisms of
735 coke growth on mordenite zeolite, Journal of Catalysis, 344 (2016) 354-364.
736 [41] M. Ibáñez, B. Valle, J. Bilbao, A.G. Gayubo, P. Castaño, Effect of operating
737 conditions on the coke nature and HZSM-5 catalysts deactivation in the
738 transformation of crude bio-oil into hydrocarbons, Catalysis Today, 195
739 (2012) 106-113.
740 [42] B. Valle, P. Castaño, M. Olazar, J. Bilbao, A.G. Gayubo, Deactivating species
741 in the transformation of crude bio-oil with methanol into hydrocarbons on a
742 HZSM-5 catalyst, Journal of Catalysis, 285 (2012) 304-314.
743 [43] R.S. Weber, M.V. Olarte, H. Wang, Modeling the Kinetics of Deactivation of
744 Catalysts during the Upgrading of Bio-oil, Energy & Fuels, 29 (2014) 273-277.

745 [44] Á. Ibarra, A. Veloso, J. Bilbao, J.M. Arandes, P. Castaño, Dual coke
746 deactivation pathways during the catalytic cracking of raw bio-oil and
747 vacuum gasoil in FCC conditions, Applied Catalysis B: Environmental, 182
748 (2016) 336-346.
749 [45] L. Gueudré, N. Thegarid, L. Burel, B. Jouguet, F. Meunier, Y. Schuurman, C.
750 Mirodatos, Coke chemistry under vacuum gasoil/bio-oil FCC co-processing
751 conditions, Catalysis Today, 257 (2014) 200-212.
752 [46] A.J. Maia, B.G. Oliveira, P.M. Esteves, B. Louis, Y.L. Lam, M.M. Pereira,
753 Isobutane and n-butane cracking on Ni-ZSM-5 catalyst: Effect on light olefin
754 formation, Applied Catalysis A: General, (2011) 58-64.
755 [47] A. Humphries, D.H. Harris, P. O'Connor, Chapter 2 The Nature of Active
756 Sites in Zeolites: Influence on Catalyst Performance, Studies in Surface
757 Science and Catalysis, 76 (1993) 41-82.
758 [48] G. Bellussi, F. Mizia, V. Calemma, P. Pollesel, R. Millini, Oligomerization of
759 olefins from Light Cracking Naphtha over zeolite-based catalyst for the
760 production of high quality diesel fuel, Microporous and Mesoporous
761 Materials, 164 (2012) 127-134.
762
763
764
765
766
767
768
769

770

771

772